REGULAR ARTICLE

Structural and optical properties of a neutral Nickel bisdithiolene complex: density functional versus ab initio methods

Fabienne Alary · Jean-Louis Heully ·
Anthony Scemama · Bénédicte Garreau-de Bonneval ·
Kathleen I. Chane-Ching · Michel Caffarel

Abstract Density functional theory (DFT) and ab initio computations are applied to examine different properties of diamagnetic, square planar neutral nickel complexes that contain two bidentate ligands derived from bis ((ethylene)-1,2-dithiolato) ligands. Geometry, vibrational spectra (IR and Raman) are well reproduced in the density functional framework whereas TD-DFT methods are clearly insufficient to reproduce absorption properties. Multiconfigurational perturbation theory based on a complete active space self-consistent field wave function, i.e. MRPT2 and MRPT4 methods, reveal the pronounced multiconfigurational character of the ground state wave function. The singlet–triplet energy gap, the energy gained from symmetry breaking and the singlet diradical character are discussed in the DFT and ab initio frameworks. The complex of interest does not display a strong singlet diradical character. This molecule having a peculiar electronic structure; strong delocalization as shown by a new electron pair localization function analysis (EPLF); exemplifies the fragility of the TD-DFT method and thus, caution should be taken in the determination of the energetic properties of such compounds.

F. Alary (✉) · J.-L. Heully · A. Scemama · M. Caffarel
LCPQ-UMR 5626-IRSAMC-118, route de Narbonne,
31062 Toulouse Cedex 07, France
e-mail: fabienne.alary@irsamc.ups-tlse.fr

B. Garreau-de Bonneval · K. I. Chane-Ching
LCC-UPR 8241-205, route de Narbonne,
31077 Toulouse Cedex 04, France

1 Introduction

Dithiolene transition metal complexes have received considerable attention in inorganic chemistry due to their unusual physical properties and electronic structures. Over the last decade, numerous experimental and theoretical studies have been performed with different metal bisdithiolenes, based on a choice of transition metals and the dithiolene ligands [1–6]. This type of complexes shows a variety of very different properties. Neutral nickel bisdithiolenes may serve as catalysts but they are also chromophores that exhibit very intense long-wavelength absorption in the visible or in the near infrared region of the electromagnetic spectrum. Therefore, they have been studied for optical data storage systems and have been considered for building supramolecular array and polymer systems in optoelectronic technology. Such versatile properties of these compounds surely underline an original electronic structure. Indeed, since 1968 a long debate has taken place on the physical oxidation state of the Nickel atom. Restricting the oxidation state of the central Ni atom to +II, three models for the electronic structures are discussed in the literature, they are schematized on Fig. 1. Schrauzer et al. [1, 7] proposed a fully delocalized structure (Structure I); Bach et al. [2] proposed that two resonance hybrid structures are necessary to describe the fundamental structure (Structure II and II') and Stiefel et al. [3] suggested that the ground state possesses a diradical character (Structure III). To choose between these different schemes one should be able to discuss on the possible biradical character of this compound. For a biradical one should find
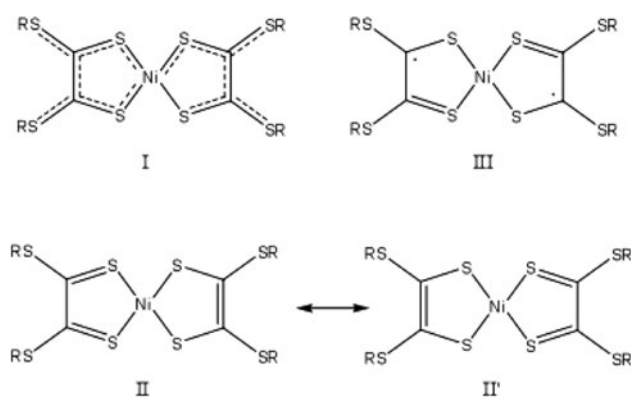
Fig. 1 I is the π-delocalized structure, II and II' are the resonance hybrids of two Lewis-Kekule-type structures, III is the Ni(II)-diradical ligand structure

one electron in two spatially well-separated and weakly coupled orbitals, whereas a closed-shell model implies only one-orbital hosting two electrons. Due to the fact that most of these complexes are diamagnetic it is experimentally difficult to distinguish between these models and thus quantum chemical calculations should bring some insights on the nature of their electronic structure.

We investigate in this work the electronic structures of a model complex $[Ni(S_2C_2(SCH_3)_2)_2]$, see Fig. 2, which should be representative of new Ni compounds, i.e. $[Ni(S_2C_2(SC_7H_{15})_2)_2]$, $[Ni(S_2C_2(SC_8H_{17})_2)_2]$, $[Ni(S_2C_2(SC_5H_{11})_2)_2]$, recently synthesized by us and which will be presented elsewhere [8]. The originality of these complexes lies in the presence of exocyclic sulfurs. To our knowledge, theoretical studies on this type of nickel bisdithiolene complexes are very scarce [9, 10].

For this purpose, we have used several methods such as Hartree–Fock (HF), Moller–Plesset (MP2), complete active space self-consistent field plus perturbation (CASSCF + MRPT2, CASSCF + MRPT4) and density functional theory (DFT). We will see that usual ab initio methods, i.e. HF and MP2 methods, contrary to DFT, have
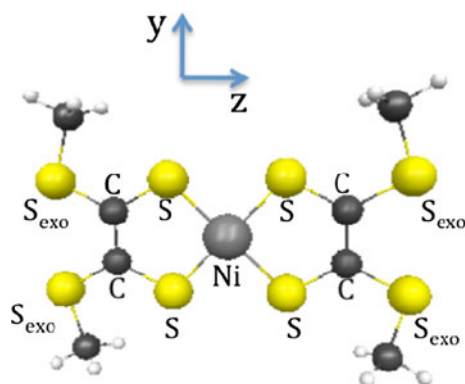
difficulties to reproduce the geometrical structure whereas the energetic picture given by DFT is not satisfactory. The absorption spectrum is particularly poorly reproduced by time-dependent density functional theory (TDDFT). We will reveal that the metal atom plays a very secondary role in the electronic structure, and that it is mostly the π system of all the sulfur atoms which is relevant. An important electronic delocalization takes place in this π system, rendering difficult the discussion of the singlet diradical character. Section 3.3 is devoted to the investigation of the nature of the electron pairing in this nickel complex. For that, we shall use a recently proposed approach, i.e. the electron pair localization function (EPLF) [11], based on the visualization of the local minimum distances between spin-like and -unlike electrons. In practice, it has been shown that such information can be encapsulated in a simple manner by defining a scalar function, the EPLF, defined in the ordinary 3D-space and taking its values in the [−1, 1] interval. The major advantages of this function describing the local pairing of electrons are twofold. First, the EPLF allows to have a direct access to the most fundamental information we are interested in: Are the electrons paired or not in the region of space we are looking at? Second, the EPLF can be easily computed using quantum Monte Carlo techniques. From a practical point of view, this is an important property since the nature of the pair localization as a function of the level of approximation considered can be investigated without being limited by the particular form of the wavefunction (one-particle expansions: Hartree–Fock, CASSCF, Valence Bond, DFT, etc.; explicitly correlated forms: Jastrow-Slater wavefunctions, geminals, etc.; almost exact: Fixed-Node Diffusion Monte Carlo, Green's Function MC, etc.). A number of applications of EPLF have been presented; they have illustrated the chemical interest of using the EPLF [11, 12]. In this work, we would like to go one step further by presenting in the computational details section a modified version of the EPLF.

2 Computational details

In the calculations, we used a methyl group to mimick the alkyl (R = heptyl, methyl-butyl, ethyl-hexyl) substituent of the S_{exo} atom. This kind of simplification has been validated by previous work [13, 14]. Electronic structure calculations were carried out using ORCA [15], Gamess [16] and PC Gamess [17] packages. In a first conventional approach, we have tested the suitability of different exchange–correlation functionals, i.e. BLYP [18, 19], OLYP [20, 21], PWP [22], TPSS [23], PBE [24, 25], RPBE [26], PBE-vdw [27], B3LYP [18], PBE0 [28], M06-L [29], M06 [20], TPSSh [30] in their ability to predict the geometry of the complex, as the X-ray coordinates of the

Fig. 2 Atom labeling scheme for nickel complex

parent molecules are known. Calculations using generalized gradient approximation are performed with a triple-ζ plus polarization basis set [Ahlrichs TZV (2df, 2pd)] [31] plus auxiliary bases [32, 33] for the hydrogen, carbon, sulfur and nickel atoms. Then calculations with hybrid functionals were performed within three schemes; (i) The M06, B3LYP, TPSSh, PBE0 were employed in combination with triple-ζ plus polarization basis set [Ahlrichs TZV (2df, 2pd)] [31] for hydrogen, carbon and sulfur atoms and the nickel atom was described by a scalar relativistic electron core potential [34] with its basis set; (ii) PBE0 was employed in combination with triple-ζ plus polarization basis set [Ahlrichs TZV (2df, 2pd)] [31] for hydrogen, carbon, sulfur and nickel atoms; relativity was treated by the ZORA method. [35]; (iii) PBE0 was employed in combination with triple-ζ plus polarization basis set [Ahlrichs TZV (2df, 2pd)] [31] for hydrogen, carbon, sulfur and nickel atoms; results shown in Table 2 show that omission of relativistic effects do not affect the quality of the geometrical parameters. These three different computational procedures are thereafter referred to as CP_1, CP_2, CP_3.

2.1 Ab initio calculations

Post Hartree–Fock calculations were performed with the CP_2 procedure with the ORCA program. The geometries used are the optimized DFT (PBE0) geometries. The multi-reference perturbation theory used two selection thresholds in order to reduce the size of the calculation. First, a selected configuration in the reference is kept if its weight is superior to 10^{-4}. Then the configurations coming from the outer space are retained if their perturbative weights are larger than 10^{-5}. Comparing such calculations with a full MRPT2, without selection, having only the two main configurations, shows that the second threshold is adequate.

The optima structures of ground state and lowest triplet state were confirmed by Hessians. The second derivatives provided the harmonic vibrational frequencies, which were not corrected for anharmonicity and additional correlation effects by scaling factors. The prediction of IR and Raman intensities were done with the PC-Gamess program with the CP_3 procedure.

2.2 Prediction of Raman intensities

The Raman activities (S_i) calculated were converted to relative Raman intensities (I_i) using the following relationship derived from the basic theory of Raman Scattering [36]

$$I_i = \frac{f(\bar{v}_0 - \bar{v}_i)^4 S_i}{\bar{v}_i[1 - \exp(hc\bar{v}_i/kT)]}$$

where $\bar{v}_0$ is the exciting frequency (in cm^{-1}), $\bar{v}_i$ is the vibrational wavenumber of the ith mode, h, c and k are the fundamental constants and f is a suitably chosen common normalization factor for all peak intensities. Herein, the conversion was carried out with $\bar{v}_0 = 15,802.8$ cm^{-1} and $T = 298$ K.

2.3 Population analysis

Atomic charges were derived by Weinhold's natural population analysis (NPA) using the natural orbital (NBO) partitioning scheme [37].

2.4 Electron pair localization function

The key point of the new pair localization indicator proposed here is that it retains essentially the same chemical information as the EPLF, while it is now computable exactly by standard (deterministic) approaches. The only condition required for exact computation is that the wavefunction is written as a sum of determinants built from one-particle molecular orbitals, a condition which is of course verified within all Hartree–Fock, post-Hartree–Fock, and DFT schemes. The EPLF [11] has been designed to describe local electron pairing in molecular systems. It is defined as a scalar function defined in the three-dimensional space and taking its values in the [−1, 1] range. It is defined as follows:

$$\text{EPLF}(\vec{r}) = \frac{d_{\sigma\sigma}(\vec{r}) - d_{\sigma\bar{\sigma}}(\vec{r})}{d_{\sigma\sigma}(\vec{r}) + d_{\sigma\bar{\sigma}}(\vec{r})}$$

where the quantity $d_{\sigma\sigma}(\vec{r})$ [resp. $d_{\sigma\bar{\sigma}}(\vec{r})$] denotes the quantum–mechanical average of the distance between an electron of spin σ located at $\vec{r}$ and the closest electron of same spin (resp., of opposite spin $\bar{\sigma}$).

The mathematical definition of these quantities can be written as

$$d_{\sigma\sigma}(\vec{r}) = \int \Psi^2(\vec{r}_1, \ldots, \vec{r}_N)$$
$$\times \left[\sum_{i=1}^{N} \delta(\vec{r} - \vec{r}_i) \min_{j \neq i; \, \sigma_j = \sigma_i} \left| \vec{r}_i - \vec{r}_j \right| \right] d\vec{r}_1 \ldots d\vec{r}_N$$

$$d_{\sigma\bar{\sigma}}(\vec{\gamma}) = \int \Psi^2(\vec{r}_1, \ldots, \vec{r}_N)$$
$$\times \left[\sum_{i=1}^{N} \delta(\vec{r} - \vec{r}_i) \min_{j \neq i; \, \sigma_j \neq \sigma_i} \left| \vec{r}_i - \vec{r}_j \right| \right] d\vec{r}_1 \ldots d\vec{r}_N$$

where σ is the spin (α or β), $\bar{\sigma}$ is the spin opposite to σ, $\Psi(\vec{r}_1, \ldots, \vec{r}_N)$ is the wave function, and N is the number of electrons.

In a region of space, if the shortest distance separating anti-parallel electrons is smaller than the shortest distance separating electrons of same spin, the EPLF takes positive values and indicates pairing of anti-parallel electrons.

In contrast, if the shortest distance separating anti-parallel electrons is larger than the shortest distance separating electrons of same spin, the EPLF takes negative values and indicates pairing of parallel electrons (which in practice never happens). If the shortest distance separating anti-parallel electrons is equivalent to the shortest distance separating electrons of same spin, the EPLF takes values close to zero and indicates no electron pairing.

The original formulation of EPLF is extremely easy to compute in the quantum Monte Carlo framework. However, it is not possible to compute it analytically due to the presence of the *min* function in the definitions of $d_{\sigma\sigma}$ and $d_{\sigma\bar{\sigma}}$. We propose now a modified version of the EPLF allowing such a possibility.

2.5 The modified EPLF

To evaluate exactly the average of the *min* function is not possible. Here, we propose to introduce a representation of this function in terms of gaussians and to construct our d-functions in a slightly different way so that the gaussian contributions can be exactly integrated out. The representation of the *min* function we are considering here is written as

$$\min_{j\neq i}\left|\vec{r}_i - \vec{r}_j\right| = \lim_{\gamma\to\infty}\sqrt{-\frac{1}{\gamma}\ln\left(\sum_{j\neq i}e^{-\gamma\left|\vec{r}_i-\vec{r}_j\right|^2}\right)}$$

and we propose to define the new modified average-distances as

$$f_{\sigma\sigma}^{\gamma}(\vec{r}) = \sum_{i=1}^{N}\delta(\vec{r}-\vec{r}_i)\sum_{j\neq i;\sigma_i=\sigma_j}^{N}e^{-\gamma\left|\vec{r}_i-\vec{r}_j\right|^2}$$

$$f_{\sigma\bar{\sigma}}^{\gamma}(\vec{r}) = \sum_{i=1}^{N}\delta(\vec{r}-\vec{r}_i)\sum_{j;\sigma_i\neq\sigma_j}^{N}e^{-\gamma\left|\vec{r}_i-\vec{r}_j\right|^2}$$

we obtain

$$\mathrm{EPLF}(\vec{r}) = \frac{\sqrt{-\frac{1}{\gamma}\ln\langle\Psi|f_{\sigma\sigma}^{\gamma}(\vec{r})|\Psi\rangle} - \sqrt{-\frac{1}{\gamma}\ln\langle\Psi|f_{\sigma\bar{\sigma}}^{\gamma}(\vec{r})|\Psi\rangle}}{\sqrt{-\frac{1}{\gamma}\ln\langle\Psi|f_{\sigma\sigma}^{\gamma}(\vec{r})|\Psi\rangle} + \sqrt{-\frac{1}{\gamma}\ln\langle\Psi|f_{\sigma\bar{\sigma}}^{\gamma}(\vec{r})|\Psi\rangle}}$$

In our definition of the modified EPLF, the parameter γ is supposed to be (very) large. In practice, if it is chosen too small, the integrals $\langle\Psi|f_{\sigma\bar{\sigma}}(\vec{r})|\Psi\rangle$ can take values larger than 1 in regions of high density. If it is chosen too large, numerical instabilities appear since the values of the integrals become extremely small. We propose to use a value of γ, which depends on the electron density $\rho(\vec{r})$ as:

$$\gamma(\vec{r}) = 100 \times (-\ln\ \varepsilon)\rho^{2/3}(\vec{r})$$

where ε is the smallest possible floating point number that can be represented with 64 bits ($\sim 2.10^{-308}$). The reason for this choice is the following. The largest possible value of the approximate shortest distance can be computed as

$$d^{\max} = \sqrt{-\frac{1}{\gamma}\log\varepsilon}$$

Substituting with $\gamma(\vec{r})$, one obtains $d^{\max}(\vec{r}) = \frac{\rho^{-1/3}(\vec{r})}{10}$. If the density in the sphere centered at $\vec{r}$ with radius $d^{\max}(\vec{r})$ is

$$d_{\sigma\sigma}(\vec{r}) \sim \lim_{\gamma\to\infty}\sqrt{-\frac{1}{\gamma}\ln\int\Psi^2(\vec{r}_1,\ldots,\vec{r}_N)\sum_{i=1}^{N}\delta(\vec{r}-\vec{r}_i)\sum_{j\neq i;\sigma_i=\sigma_j}^{N}e^{-\gamma\left|\vec{r}_i-\vec{r}_j\right|^2}d\vec{r}_1\ldots d\vec{r}_N}$$

$$d_{\sigma\bar{\sigma}}(\vec{r}) \sim \lim_{\gamma\to\infty}\sqrt{-\frac{1}{\gamma}\ln\int\Psi^2(\vec{r}_1,\ldots,\vec{r}_N)\sum_{i=1}^{N}\delta(\vec{r}-\vec{r}_i)\sum_{j\neq i;\sigma_i\neq\sigma_j}^{N}e^{-\gamma\left|\vec{r}_i-\vec{r}_j\right|^2}d\vec{r}_1\ldots d\vec{r}_N}$$

Note that these new definitions of the average-distances are different from the previous ones essentially because

$$\ln\langle X\rangle \neq \langle\ln X\rangle \tag{1}$$

where X denotes the sum $\sum_j e^{-\gamma\left|\vec{r}-\vec{r}_j\right|^2}$ and the symbol $\langle\ \rangle$ denotes the quantum average. Remark that the equality in Eq. 1 is almost reached when the fluctuations of X are small. In our applications, it seems that we are not too far from this regime and we have thus systematically observed that both definitions of the d-functions lead to similar EPLF landscapes. Now, introducing

considered constant, this sphere contains on average 0.004 electron. Therefore, the value of $\langle\Psi|f^{\gamma}(r)|\Psi\rangle$ is very unlikely to exceed 1, and the value of γ will also be sufficiently large in the valence regions.

2.6 Application of the new EPLF to simple cases

To illustrate the results obtained with the new EPLF, we present the results obtained for three simple systems: the C–C single bond in C_2H_6, the C = C double bond in C_2H_4 and the CH_3 radical in Figs. 3, 4.
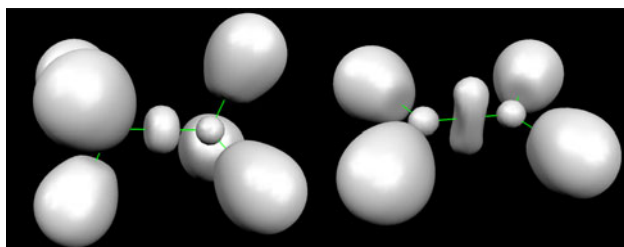
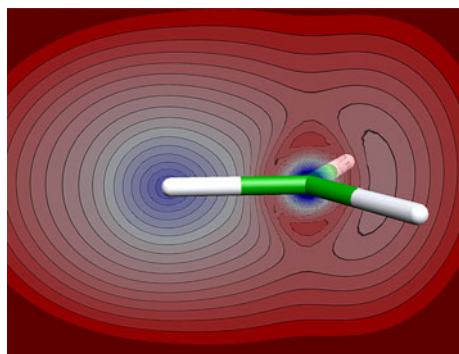**Fig. 3** The C_2H_6 and the C_2H_4 molecules EPLF = 0.12

Fig. 4 EPLF of the CH_3 radical. The values are plotted in the plane perpendicular to the molecular plane, containing a hydrogen and the carbon nuclei. *Blue values* indicate large values of EPLF and *red values* correspond to low values of EPLF

For the closed-shell systems, the displayed isosurface is EPLF = 0.12. The images obtained are similar to what would be obtained with Becke and Edgecombe's electron localization function (ELF) [38]: one domain for each C–H bond, one domain for each carbon 1s shell, and one domain corresponding to the C–C bond, with a maximum value located at the center of the molecule. Indeed in closed shell systems the anti-parallel electron pairs are localized where the electrons are localized. In the CH_3 radical, the topologies of the ELF and the EPLF are different: the ELF exhibits maxima where the unpaired electron is localized and the EPLF exhibits minima since the electron pairing is minimal. As electron pairs can be identified by maxima of the EPLF and unpaired electrons can be identified by minima, the EPLF is a very useful tool to understand electronic structure, especially in open-shell systems.

3 Results and discussion

3.1 Characterization of the ground state of [Ni $(S_2C_2(SCH_3)_2)_2$]

3.1.1 HF and MP2 calculations

In a preliminary study, we used the MOPAC program with the PM6 parameters [39]. Two geometries, quasi degenerate

Table 1 Selected bond lengths (Å) of the complex

	Exp	HF[a]	HF[b]		HF + OPT[a]	MP2[b]
Ni–S	2.13	2.27	2.23	2.41	2.21	2.00
C–C	1.37	1.41	1.51	1.33	1.40	1.39
S–C	1.70	1.69	1.72	1.78	1.66	1.70
C–S$_{exo}$	1.75	1.75	1.63	1.76	1.72	1.74

[a] Geometry optimization under D_2 symmetry constraint

[b] Geometry optimization without symmetry constraint

in energy, were found. One shows a symmetrical structure (D_{2h}) in relatively good agreement with experimental data (Structure I of Fig. 1). The other geometry corresponds to one of the unsymmetrical Lewis-Kekule-type structures as proposed by Bach et al. [2] (Structure II or II' of Fig. 1). A similar result is obtained at the HF level.

Two minima separated by 5 kcal/mol were found, the symmetrical Kekule form being the lowest. Their geometrical parameters are given in Table 1 (third and fourth column). As the experimental parameters give a totally symmetrical geometry, we see that HF is unable to give any information on this system. For the symmetrical structure the Ni–S bond length is particularly poorly reproduced. We tried to improve this rather bad HF structure by using MP2 or by adding a DFT correlation potential (OPT) [40] to the HF potential. As seen in Table 1, the correlation potential does improve the HF result but not sufficiently. The MP2 theory reduces the too large Ni–S bond length but by far too much. Similar MP2 results can been seen [9] for related complexes. One can therefore conclude that a large amount of correlation effects should be taken into account and surely higher correlated treatment such as CCSD(T) would be necessary if one wants to use ab initio methods.

3.1.2 DFT calculations with non-hybrid GGA functionals

Density functional theory methods turned out to be more suited for the structural study of this complex. We first tried with different non-hybrid GGA functionals. The results are presented in Table 2. Though quite different in their foundations, all these functionals give similar results, which are in far better agreement with experiment than ab initio results. All the bond lengths are reasonably described except the Ni–S length, which remains a little too long. The M06-L gives the best results whereas BLYP gives the worst. All geometries are of C_{2v}, D_{2h} or D_2 symmetry depending solely on the position of the methyl group, so we pursued this study in the D_2 symmetry group.

### 3.1.3 DFT calculations with hybrid functionals

In the next step, we used hybrid functionals and studied the influence of the scalar relativistic effects. Comparing

Table 2 Selected bond lengths (Å) of the complex

	Exp	BLYP[a]	OLYP[a]	PWP[a]	TPSS[a]	RPBE[a]	PBE[a]	PBE-vdw[a]	M06-L[b]
Ni–S	2.13	2.18	2.16	2.15	2.15	2.17	2.15	2.15	2.15
C–C	1.37	1.41	1.41	1.41	1.40	1.41	1.40	1.40	1.39
S–C	1.70	1.73	1.71	1.72	1.72	1.73	1.72	1.72	1.70
C–S_{exo}	1.75	1.78	1.76	1.76	1.76	1.77	1.76	1.76	1.74

[a] Geometry optimization without symmetry constraint

[b] Geometry optimization under D_2 symmetry constraint

Table 3 Selected bond lengths (Å) of the complex

	Exp	B3LYP[a]	TPSSh[a]	M06[a]	PBE0[a]	PBE0 + Zora[a]	PBE0 + ECP[a]
Ni–S	2.13	2.17	2.14	2.15	2.14	2.13	2.13
C–C	1.37	1.40	1.40	1.40	1.40	1.40	1.40
S–C	1.70	1.71	1.71	1.70	1.70	1.70	1.70
C–S_{exo}	1.75	1.76	1.76	1.75	1.74	1.75	1.74

[a] Geometry optimization under D_2 symmetry constraint
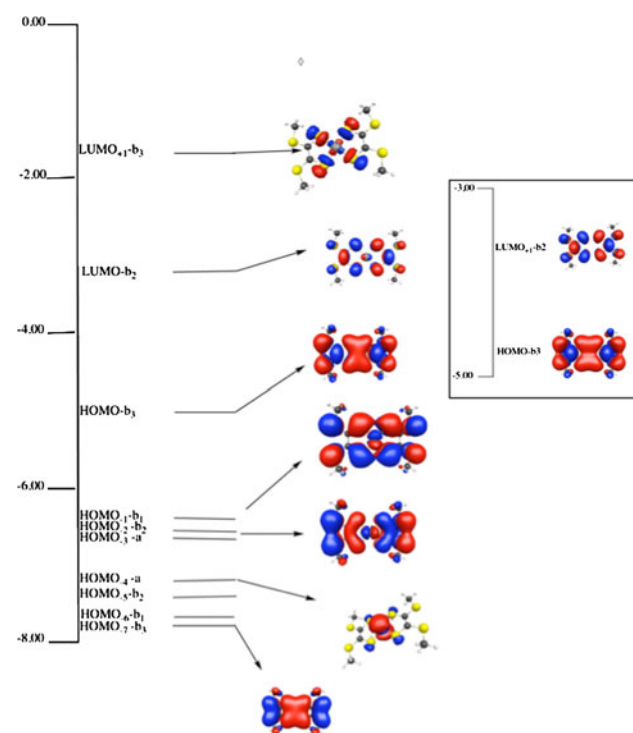
Fig. 5 Frontier orbitals of the complex in the closed-shell state and, in the inset corresponding HOMO-LUMO of the two planar bidentate ligands alone

Tables 2, 3 shows that the HF part in the functionals has a rather limited but favorable effect. The LYP functional leads to a slight improvement but the Ni–S bond length remains too long. PBE0 performs quite well for this distance. One can see that for all functionals the C–C bond length is too large but always indicates a double bound.

The S–C bond lengths all range between single (1.83 Å in methyl mercaptan) and double (1.6 Å in thioketone) bond length. The values of 1.70 for the C–S and 1.75 Å for the C–S_{exo} bond length are comparable to those of the delocalized C–S bond in thiophene (1.73 Å). Consequently, the ground state appears to be a completely π-delocalized system. Relativity was included either by the ZORA method or by using a relativistic pseudo potential. The two methods give the same results and comparing with a non-relativistic calculation, one can conclude that negligible relativistic effects appear (bond length contraction of 0.01 Å for the Ni–S bond). This slight effect is the same as observed by Romaniello et al. [41]. The low atomic number of the S and Ni atoms but also the nature of their bonds, which is very weak, explains this result.

Symmetries, relative energies and schematic diagram of the frontier Kohn–Sham orbitals of the complex and of the ligands cage are shown in Fig. 5. Ligand valence orbitals lie at higher energy than the Ni d orbital manifold. This exemplifies the "inverted" bonding description of such non-innocent ligands. In the closed-shell ground state, the HOMO is an orbital overwhelmingly ligand in character. This HOMO is shown to be delocalized over the sulfur backbone. The LUMO is mainly $S(3p_x)$ in character and contains non-negligible antibonding interactions between Ni ($3d_{xz}$) and ligand b_2 orbital. The fact that the sulfur atoms tend to delocalize their electrons can also be seen in the HOMO-1, HOMO-2 and HOMO-7 orbitals. In all those orbitals, no clear bonding contributions of the Ni d orbitals can be seen. We have performed the same calculation but removing the Ni atom (see inset of Fig. 5): the orbitals are almost the same so the electronic structure seems to be only governed by the ligands. The NPA gives some information

Table 4 Selected PBE0 vibrational frequencies ($\bar{\nu}_{cal}$) compared to experimental frequencies ($\bar{\nu}_{exp}$)

Assignment	$\bar{\nu}_{Ni-S} + \bar{\delta}_{C-S_{exo}-C}$	$\bar{\nu}_{C-S}$		$\bar{\nu}_{C-S}$	$\bar{\nu}_{C-C}$
$\bar{\nu}_{cal}$ (cm^{-1})	494	965		990	1286
$\bar{\nu}_{exp}$ (cm^{-1})	500		980		1300

Assignment for major contribution

on the charges on the atoms. A valence population of 9.39 is given for Ni with a formal configuration $3d^9 4 s^{0.5}$. These values are compatible with a formal +II oxidation state for the metal atom as discussed by Bachler [42]. The charge excess over the formal d^8 configuration is explained if one looks at the NBO.

One finds orbitals between sulfur and nickel, with 75% weight on the sulfur, which indicates small charge transfer from the ligands to the metal leading to a weak covalent bonding. The internal carbons have a charge of 0.42 indicating an excess of one electron on each C–C bond. The C–C bond length of 1.40 Å (exp 1.37), almost equivalent to the C–C bond length of benzene (1.397), indicates that delocalization occurs in each cycle.

3.1.4 IR spectrum

The vibrational spectra of this model molecule have a limited number of modes because of its high symmetry. Among them, only four modes have a reasonable intensity (we have neglected the C–H vibrations). Absorption vibrational frequencies for [Ni(S$_2$C$_2$(SCH$_3$)$_2$)$_2$] agree well with experimental values and with previously reported values [9, 43, 44]. Representations of these normal modes are given in Table 4. At 1286 cm^{-1}, one finds the most intense one by far, and this is the antisymmetric stretching mode of the C–C units. Following this mode would lead to the two resonance structures mentioned in Fig. 1 as Structures II and II'. Then two modes at 990 and 965 cm^{-1} describe the vibrations of the C atom with the exocyclic and ring sulfurs. Finally, the vibration between the metal and the sulfurs has low intensity and is situated just below 500 cm^{-1}. The $\bar{\nu}$(C = C) stretching vibration is downshifted compared with usually reported values, while $\bar{\nu}$(C − S) and $\bar{\nu}$(Ni − S) stretching are upshifted. Those trends indicate a strengthening of the Ni–S bond upon delocalization. This behavior is in agreement with the previously discussed changes of structural parameters.

3.1.5 Raman spectrum

The results are presented in Table 5 and show a very good agreement with experimental data. The most intense calculated frequencies deviate by 50 cm^{-1} without scaling.

Our assignment is, in general, similar to those proposed for neutral bisdithiolene complexes in previous scarce works [45, 46]. The strong mode at 267 cm^{-1} is attributed to C = C–S$_{exo}$ stretching mode. The frequency at 305 cm^{-1} is an in-phase rocking motion, which leads to a deformation of the whole molecule. The low intensive mode at 378 cm^{-1} corresponds to a combination of Ni–S stretching bond and C = C–S bending mode. The modes at 1108, 990, 494 and 748 cm^{-1} correspond to C–S bond stretching modes. In agreement with the assignment proposed by [46] the strong mode at 496 cm^{-1} consists of a combination of C = C and C–S bond stretching mode of the S$_2$C = S$_2$C fragment with a major contribution of C–S stretching mode. Those regions are characteristic for those types of vibrations. The weak mode at 748 cm^{-1} is a characteristic mode, which consists of C$_{CH_3}$ − S$_{exo}$ bond stretching mode. The higher mode at 1108 cm^{-1} corresponds to a out-of-phase combination of C–S stretching modes. As observed in the IR Spectrum, the C–C stretching mode is the only one which is not mixed with other vibrations. Computed Raman Spectrum shows the same trend as IR spectrum. For instance, the Ni–S stretching mode is upshifted due to the delocalization of the π-system of the ligand. A complete analysis of experimental of the Raman spectra of the real complexes will be presented elsewhere [8].
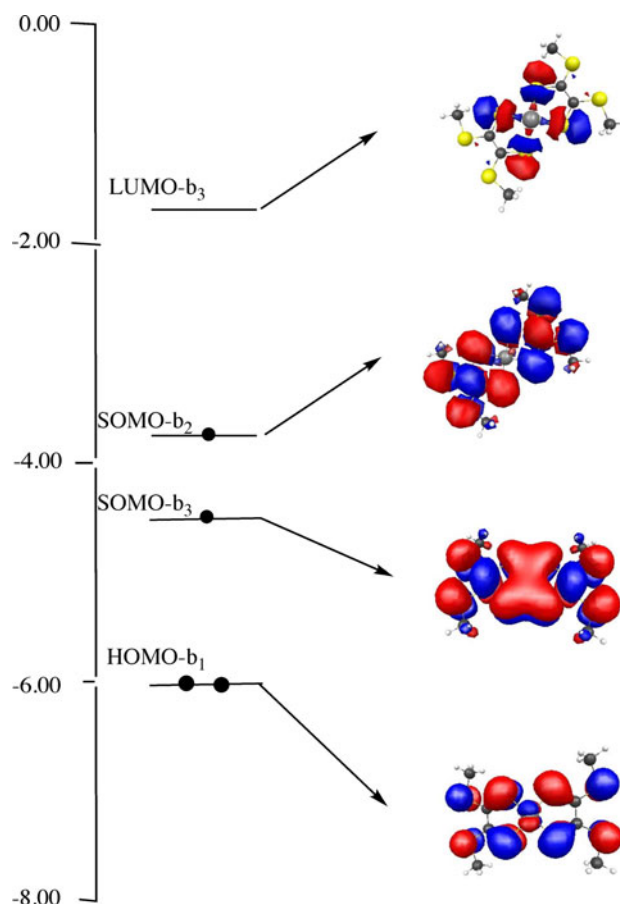
3.2 Characterization of the excited triplet state

The geometry of the lowest triplet excited state was optimized and vibrational frequencies were computed. Such a calculation can confirm that the complex is diamagnetic but also give information on the corresponding singlet state, which should be important for the description of a possible diradical character.

Table 5 Comparison of the experimental and calculated Raman frequencies of the complex in cm^{-1}

Exp	PBE0	Assignment	
230(s)	267(s)		$\bar{\delta}_{C=C-S_{exo}}$
308(w)	305(w)		$\bar{\delta}_{C=C-S_{exo}} + \bar{\delta}_{C=C-S}$
380(vs)	378(vs)		$\bar{v}_{C-Ni} + \bar{\delta}_{C=C-S}$
496(s)	494(s)		$\bar{v}_{C-S}$
760(w)	748(w)		$\bar{v}_{C-S}$
940(vs)	990(vs)		$\bar{v}_{C-S}$
1,065(w)	1,108(w)		$\bar{v}_{C-S}$
1,411(w)	1,398(w)		$\bar{v}_{C-C}$

w weak, *s* strong, *vs* very strong

Fig. 6 Simplified MO scheme for the lowest triplet state

Table 6 Selected bond lengths (Å) of the complex in its lowest state triplet

Bond length	PBE0
Ni–S	2.18
C–C	1.40
S–C	1.70
C–S$_{exo}$	1.73

As can be seen on Fig. 6, the LUMO of the closed-shell ground state becomes the SOMO in the triplet state. Bond lengths for the optimized lowest triplet state structure are included in Table 6. The main geometric change compared to the ground state is the slight lengthening of the Ni–S bond lengths from 2.14 to 2.18 Å. This change is a consequence of the promotion of an electron in the LUMO orbital, which has antibonding character between the $3d_{xz}$ of the metal center and the ligand orbital.

An analysis of the spin density (alpha–beta difference) shows that the two valence electrons are delocalized over the four internal carbons (0.17) and the four internal sulfurs (0.19). This triplet state is rather low in energy, ca. 4.7 kcal/mol above the ground state. This calculation was

Table 7 Computed TD-DFT wavelengths (nm) and vertical excitation energies (eV) and oscillator strengths (f) for singlet states with $f > 0.01$ in terms of single molecular orbital excitations

λ, nm (eV)	Principal configuration	State labeling	f
818 (1.51)	HOMO (b_3) $\rightarrow$ LUMO (b_2)	B_1	0.354
341 (3.63)	HOMO$_{-7}$ (b_3) $\rightarrow$ LUMO(b_2)	B_1	0.085
297.4 (4.17)	HOMO$_{-8}$ (b_1) $\rightarrow$ LUMO$_{+1}$ (b_3)	B_2	0.153
	HOMO (b_3) $\rightarrow$ LUMO$_{+3}$ (b_1)		
255 (4.86)	HOMO$_{-5}$ (b_2) $\rightarrow$ LUMO$_{+1}$ (b_3)	B_1	0.741
238.5 (5.19)	HOMO$_{-8}$ (b_1) $\rightarrow$ LUMO$_{+1}$ (b_3)	B_2	0.4
	HOMO$_{-9}$ (a) $\rightarrow$ LUMO (b_2)		
224 (5.53)	HOMO$_{-3}$ (a) $\rightarrow$ LUMO$_{+3}$ (b_1)	B_1	0.476
	HOMO$_{-1}$ (b_1) $\rightarrow$ LUMO$_{+5}$ (a)		

| 1.42 | 0.47 |

Fig. 7 Representation of the first two natural orbitals for the CAS (2,4) with their respective population

performed with a restricted Kohn–Sham method (RODFT), so an unrestricted method should lower this energy further. However, all the nickel bisdithiolene compounds are known to be diamagnetic, thus this triplet should lie above the closed-shell ground state. Even though the geometry of the singlet state corresponds very well with the experimental results, some doubts can be cast over the energy given by this DFT method. We have thus used the CASSCF + MRPT2 method to obtain the ground state singlet–triplet energy difference. With such a method one cannot optimize the geometry, therefore, the calculation was performed at the PBE0 ground state geometry. We chose a small active space containing the HOMO and the three next orbitals, i.e. CAS (2,4). It turned out that the ground state needs two configurations to be properly described. The normal configuration having two electrons in the HOMO has only a coefficient of 0.84, whereas the second configuration with two electrons in the LUMO (a di-excited configuration) has a coefficient of −0.53. The natural orbital occupations of the two orbitals involved are 1.42 and 0.47. The presence of these two configurations built on two molecular orbitals, one being antisymmetric (*XY* plane) with respect to the other, implying possible separation of charges will be discussed in Sect. 3.5. On contrary, the triplet state is very well described by a single configuration. It should be noted that for the ground state the natural orbitals coming from the CASSCF are totally similar to those coming from the DFT method as can be seen on Fig. 7.

Therefore, it appears that the ground state is more difficult to describe than the excited state. After inclusion of the dynamical correlation by the MRPT2 method, the triplet is found 23 kcal/mol above the ground state. This is in sharp contrast with the DFT result. During the geometry optimization by the DFT method, only 2 kcal/mol were gained for the triplet. So we can conclude that the triplet is about 20 kcal/mol above the ground state. The difficulty of
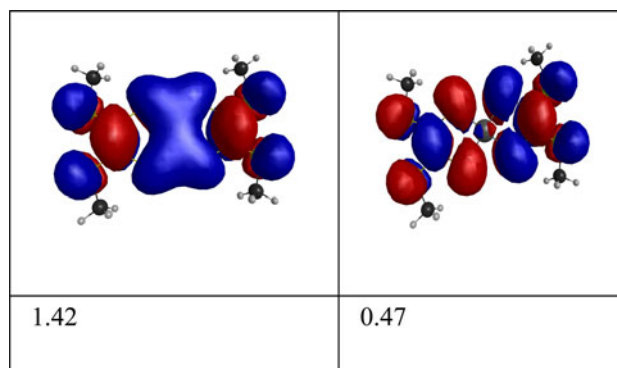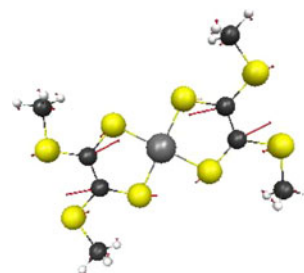
Fig. 8 Schematic representation of the C–S vibration mode in the triplet ground state

the DFT method to describe the energetics of this molecule will be also encountered in the study of the absorption spectra (Sect. 3.4).

The vibrational spectra for the lowest triplet is very different from the one of the ground state. The most intense mode is now a vibration situated at 1097 cm^{-1}. As can be seen on Fig. 8, this is a predominantly in-phase combination of antisymmetric C–S vibration stretching, affecting mostly the C–S distances. In the experimental spectra of the real complexes the most intense modes appear around 1300 cm^{-1}, which shows unambiguously that the closed-shell ground state is the one observed.

3.3 Application of new EPLF approach to the Nickel complex

For both the singlet and the triplet states of the complex, the EPLF was computed using the PBE0 determinant, at the equilibrium geometry of the singlet.

3.3.1 Singlet state

The isosurface 0.094 of the EPLF is displayed on Fig. 9. This figure shows the domains where electron pairing is predominant. One can identify the bonding region between
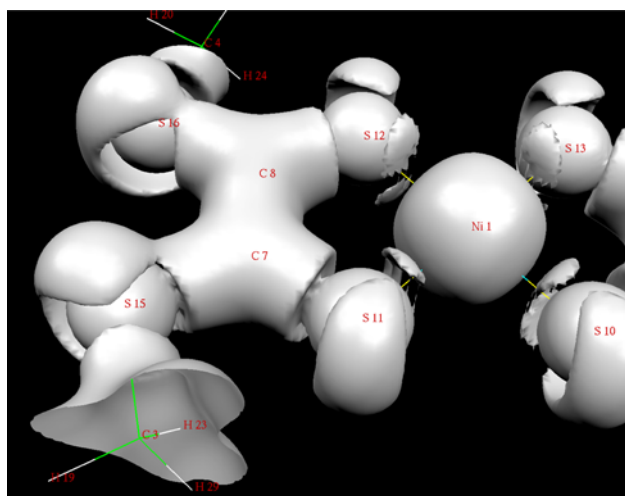
Fig. 9 Isosurface EPLF = 0.094 of the singlet state of the Nickel complex
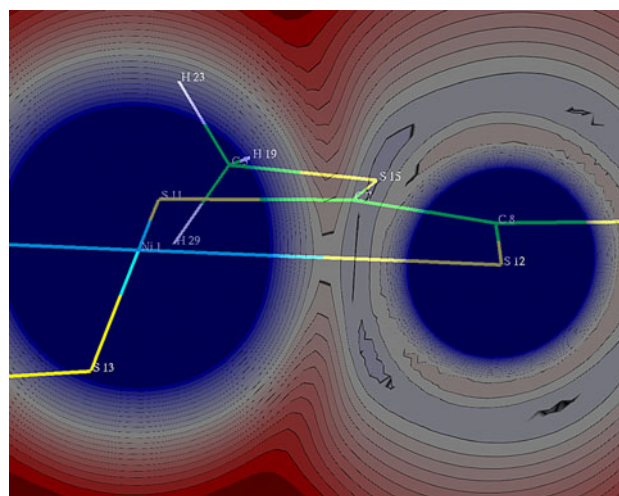

Fig. 10 EPLF of the singlet state of the Nickel complex. The values are plotted in the plane perpendicular to the molecular plane, containing two Sulfur and the Nickel nuclei. *Blue values* indicate large values of EPLF and *red values* correspond to low values of EPLF

the carbon atoms, the lone pairs of the sulfur atoms, and core domains of the sulfur and nickel atoms.

The first surprising result is that, for this particular isosurface value, the lone pair domains of the S_{exo} atoms are connected to the C–C bond domain, unlike the lone pair domains of the inner sulfur atoms. This can be interpreted as a larger delocalization between the carbon atoms and the S_{exo} atoms than between the carbon atoms and the inner sulfur atoms.

One can also note that the lone pairs of the S atoms contribute significantly to the Ni–S bond, as the EPLF exhibits a slight maximum value along the Ni–S axis, and two more distinct maxima out of the molecular plane (Fig. 10).

3.3.2 Triplet state

The calculated EPLF grid of the triplet state is very similar to the EPLF grid of the singlet. If the alpha electrons were localized, we would have found minima of the EPLF where these electrons are localized. As the EPLF grids are almost the same, we conclude that these two electrons are not localized. To be able to visualize where these two electrons reside, we computed the function $\Delta EPLF = EPLF_{Triplet} - EPLF_{Singlet}$ and plotted the isosurface $\Delta EPLF = 0.001$ (Fig. 11).

This Fig. 11 shows the tiny differences between the EPLF grids of the singlet and the triplet: there is a slight decrease of the EPLF values of the EPLF from the singlet to the triplet next to the carbon atoms (in red), which makes us believe that the two unpaired electrons are delocalized in these eight domains. We can also note that the electron pairing has slightly changed in the d electrons of the Nickel.

3.4 Absorption spectra

It has been well established that the transition energies calculated by the TDDFT method are usually comparable in accuracy to those calculated by the higher-level configuration interaction methods. Some satisfactory results have been obtained with similar species [41]. On the basis of the ground state structure, the TDDFT method was used to reproduce the absorption spectra. The nature of the orbitals and the electronic transitions involved in the absorption spectrum were studied by means of TDDFT/PBE0 calculations. Neutral Nickel bisdithiolene complexes have unique electronic spectra with intense absorptions occurring in the NIR region. These complexes show, whatever solvents used, a strong absorption band peaking around 1,006 nm (1.23 eV) and a weaker one near 340 nm (3.64 eV) [46]. The spin-allowed singlet–singlet electronic transitions calculated with the TDDFT method are shown in Table 7.

If one focuses on the two experimental transitions, we see that the first one is very poorly reproduced (shifted by 0.28 eV) whereas the second one seems correct, though with a rather small oscillator strength. If one looks at the orbitals involved in these transitions, they are rather similar. Both excitations mainly transfer electrons from the sulfur atom to the C–C bonds without participation of the metal. These transitions are of the type Inter ligand Charge Transfer. The problem with the low-energy excitation can be detected by looking at the coefficients of the configurations describing the multi-determinantal wave function of the excitation state. The coefficient HOMO to LUMO is ca. 1 whereas the coefficient coming from the Random Phase Treatment LUMO to HOMO is −0.30, this is a strong

Fig. 11 Isosurfaces
ΔEPLF $= -0.001$ (in *red*) and
ΔEPLF $= +0.001$ (in *white*) of
the Nickel complex
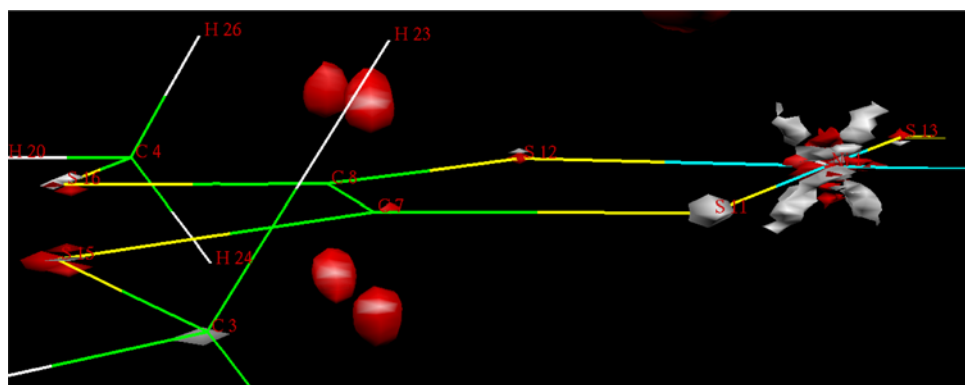
indication that the transition is not well described in the TDDFT formalism. For comparison purposes, in the case of the higher energy excitation, HOMO-7 to LUMO is 0.946 and LUMO to HOMO-7 is -0.07! If one performs the calculation once again but using the Tamm Dancoff approximation, one obtains 608 nm instead of 818 nm for the first transition, and for the second 343 nm instead of 341 nm. Therefore, the TDDFT method is unable to describe the first transition. This is certainly related to the multiconfigurational character of the ground state as discussed in the preceding section. In order to get convincing results we experimented ab initio methods again. First, we considered a (2,4) CASSCF + MRPT2, as in the treatment of the triplet state. The first singlet excited state is very well described by one configuration ($c = 0.99$). The energy of the transition from the ground state is now 925 nm, which is a large improvement but still far from the experimental result. To improve this result further, we used the MRPT4 method of Neese [15] as implemented in ORCA. This method allows one to use much larger active space and to add higher order correlation effects on the selected configurations. In our case, we selected the two HOMOs and the six LUMOs, i.e. CAS (4,8). The result for the first transition is now 999 nm, in very good agreement with the experimental result. This shows that considerable correlation effects take place. With this method, we have also obtained the energy of the triplet state, which is now ca. 10 kcal/mol above the ground state.

3.5 On the possible singlet diradical character

Following the analysis of Bachler [42], we shall discuss the diradical character of this compound. Two methods can be used to obtain an index for this character. The first one is based on a CASSCF calculation of the ground state. We have seen in Sect. 3.2 that the ground state wave function is described mainly by two determinants : a closed-shell determinant and a doubly excited determinant. These two determinants differ by one orbital, which is the antisymmetric counterpart of the other. By making a rotation

between those two orbitals one can get a localized description where the charges are on the left or on the right part of the molecule. Because the coefficients of the two configurations are different, one can achieve only a partial separation of charge. Separation of charges implies the possibility to form a singlet open-shell state radical, or to have a biradical character. As shown by Bachler [42] the coefficient of the di-excitation (c_d), in the description of the closed-shell state, is a direct measure for the singlet diradical character. They propose the following radical (rad) index, n_{rad}:

$$n_{rad} = 100|c_d|\sqrt{2}$$

In our case, $c_d = -0.5344$ gives an index of 75.6%. Comparison with other similar compounds studied by Bachler [42] shows that this index is not very high. This is certainly related to the occupation numbers of the natural orbitals of the CASSCF: 1.42 for the HOMO, 0.57 for the LUMO. The diradical character is given by only half one electron. Such an index should be interpreted as the measure of the propensity of the "formally" closed-shell state to adopt an open shell form. This is thus also a measure of the possible reactivity of this complex with true radicals. The second method is based on a DFT calculation. In this method one applies the broken symmetry formalism of Noodleman [47]. By allowing a violation of the spatial and spin symmetries, a spatial separation is introduced if the molecule presents a diradical character. One condition should be respected: the energy of this symmetry-broken unrestricted DFT solution should be lower than the restricted DFT solution. If the unphysical broken-symmetry solution, characterized by its wave function Ψ(b) and its energy E(b), is lower than the physical symmetry solution, this is a strong indication that the molecule tends to adopt a diradical configuration. In our case, we obtained almost the same energy for the restricted and broken unrestricted solutions. The diradical character is not sufficiently pronounced to produce a spontaneous symmetry breaking. We can conclude that this molecule has a low diradical character.

Nevertheless, we have used this broken-symmetry solution to compute the open-shell singlet and the triplet
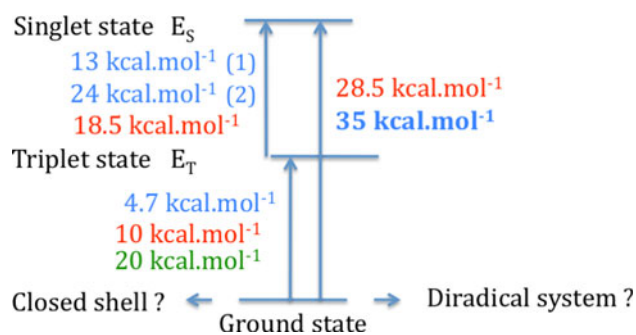
Fig. 12 Comparison of the energetics of the first excited states computed with different methods. In *blue*, values obtained in DFT framework, RODFT, TDDFT (*bold*) and broken symmetry calculations with the corresponding equation for estimation of the $E_S - E_T$ gap. In *red*, values obtained with CASSCF (4,8) + MRPT4 calculations. In *green*, values obtained with CASSCF (2,4) + MRPT2 calculations

state gap, i.e. $E_S - E_T$. We have used two formulas to calculate the energy gap:

$$E_S - E_T = E(b) - E(T) \quad (1)$$

$$E_S - E_T = \frac{2(E(b) - E(T))}{2 - \langle \psi(b) | S^2 | \psi(b) \rangle} \quad (2)$$

In our case, the calculated $\langle \psi(b) | S^2 | \psi(b) \rangle$ value was found to be 1.

It can be seen from Fig. 12 that the broken symmetry approach gives reasonable results for the calculation of the energy difference between the first triplet and the open-shell singlet as compared with the ab initio approach.

If one now returns to the description of the lower energy absorption line, we can draw some conclusions on the usability of the broken symmetry approach in the description of the excited states of this complex. Two formulas have been used to obtain the energy gap between the excited triplet and singlet states. Equation 1 should be used in the strong coupling case, which does not correspond to our case. Indeed this formula gives a transition at 0.78 eV to be compared to the experimental value of 1.23 eV. Equation 2, which is a more general formula, takes into account the spin polarization of the inner closed shells. It gives a transition at 1.256 eV in good agreement with the ab initio and experimental results. Therefore, in our case, the DFT method is able to predict the right transition energy whereas TD-DFT fails. TD-DFT is known to be inappropriate in the presence of strong charge separation. Our results tend to indicate that the TD-DFT method also encounters problems with strongly delocalized systems.

4 Conclusion

The present work has led to a detailed description of the electronic structure of the model complex [Ni(S$_2$C$_2$

(SCH$_3$)$_2$)$_2$]. Very different aspects of those complexes have been studied such as the electronic structure (geometries, charges delocalization), vibrations (IR and Raman Spectra) and excited states (absorption spectra). All the information gained by these studies lead to the same conclusions: the electronic structure adopted by this complex is strongly delocalized. However, the originality of this complex is caused by the presence of the $S_2C = CS_2$ fragment. Indeed, the complex has two possibilities for delocalization, one being delocalization around the S_{exo}-C–C-S_{exo} part, the second being delocalization in the ring, i.e. Ni-S–C–C–S, as encountered in most of nickel bisdithiolene complexes. It seems that the complex adopts the first possibility as shown by an electron pair localization analysis. This system shows a certain propensity to have a biradical character, modest compared with other bisdithiolene complexes, but sufficient to indicate that reactivity with true radicals should be possible. Concerning the ability of the different theoretical methods to reproduce experimental results, DFT succeeds very well to describe all geometrical aspects (geometries, vibrations), while TD-DFT fails to reproduce the absorption spectrum. This is certainly due to the multiconfigurational aspect of the ground state and due to the delocalized character of its electronic structure. On the contrary, ab initio methods (MP2) are not successful in reproducing the geometry but give a good description of the absorption spectrum, provided the MRPT4 method is used.

References

1. Schrauzer GN, Mayweg VP (1965) J Am Chem Soc 87:3585–3592
2. Bach AL, Holm RH (1966) J Am Chem Soc 88:5201–5209
3. Stiefel EI, Waters JH, Billig E, Gray HB (1965) J Am Chem Soc 87:3016–3017
4. Herman ZS, Kirchner RF, Loew GH, Mueller-Westerhoff UT, Nazzal A, Zerner M (1982) Inorg Chem 21:46–56
5. Lim BS, Fomitchev V, Holm RH (2001) Inorg Chem 40:4257–4262
6. Herebian D, Wieghardt KE, Neese F (2003) J Am Chem Soc 125:10997–11005
7. Schrauzer GN (1969) Acc Chem Res 2:72–80
8. Chane-Ching K, Garreau-de Bonneval B, Bui TT, Jacob KJ, Duhayon C, Alary F, Valade L (2009) Synthesis X-ray crystal structures, optical properties and modeling data of two new neutral bis(1,2-dithiolene) nickel complexes (in preparation)
9. Lauterbach C, Fabian J (1999) Eur J Inorg Chem 1995–2004
10. Wang R (2006) Internal report of Fairport High School. Fairport, NY
11. Scemama A, Chaquin P, Caffarel M (2004) J Chem Phys 121:1725–1735
12. Scemama A, Caffarel M, Ramirez-Solis A (2009). doi: 10.1021/jp902028g
13. Pyykkö P (2004) Angew Chem Int Ed 43:4412–4456
14. Carra C, Scaiano JC (2008) Eur J Org Chem 4454–4459

15. Neese F (2007) ORCA: an ab initio DFT and semiempirical SCF-MO package, University of Bonn, Bonn, Germany
16. Schmidt M, Baldridge K, Boatz J, Elbert S, Gordon M, Jensen J, Koseki S, Matsunaga N, Nguyen KA, Su S, Windus T, Dupuis M, Montgomery J (1993) J Comput Chem 14:1347
17. Nemukhin AV, Grigorenko BL, Granovsky AA (2004) Molecular modeling by using the PC GAMESS program: from diatomic molecules to enzymes. Moscow Univ Chem Bull 45:75
18. Becke AD (1988) Phys Rev A 38:3098–3100
19. Lee CT, Yang WT, Parr RG (1988) Phys Rev B 37:785–789
20. Handy NC, Cohen AJ (2001) Mol Phys 99:403–412
21. Perdew JP, Chevary JA, Vosko SH, Jackson KA, Pederson MR, Singh DJ, Fiolhais C (1992) Phys Rev B 46:6671–6687
22. Zhao Y, Truhlar DG (2006) J Chem Phys 125:194101(1)–194101(18)
23. Tao J, Perdew J, Staroverov V, Scuseria G (2003) Phys Rev Lett 91:1–146401
24. Perdew JP, Burke K, Ernzerhof M (1996) Phys Rev Lett 77:3865–3868
25. Perdew JP, Burke K, Ernzerhof M (1997) Phys Rev Lett 78:1396
26. Hammer B, Hansen LB, Nørskov J (1999) Phys Rev B 58:7413–7421
27. Grimme S (2006) J Chem Phys 124:034108
28. Adamo C, Barone V (1999) J Chem Phys 110:6158–6170
29. Zhao Y, Schultz NE, Truhlar DG (2006) J Chem Theory Comput 2:364–382
30. Staroverov V, Scuseria G, Tao J, Perdew J (2003) J Chem Phys 119:12129–12137
31. Schäfer A, Horn H, Ahlrichs R (1992) J Chem Phys 97:2571–2577
32. Eichkorn K, Treutler O, Ohm H, Haser M, Ahlrichs R (1995) Chem Phys Lett 240:283–289
33. Eichkorn K, Weigend F, Treutler O, Ahlrichs R (1997) Theor Chem Acc 97:119–124
34. Dolg M, Stoll H, Preuss H, Pitzer RM (1993) J Phys Chem 9:5852–5859
35. Van Wüllen C (1998) J Chem Phys 109:392–399
36. Polavarapu PL (1990) J Phys Chem 94:8106–8112
37. Reed AE, Curtiss LA, Weinhold F (1988) Chem Rev 88:899–926
38. Becke AD, Edgecombe KE (1990) J Chem Phys 92:5397
39. Stewart JJP (2007) J Mol Model 13:1173–1213
40. Tsuneda T, Hirao K (1997) Chem Phys Lett 268:510–520
41. Romaniello P, Aragoni MC, Arca M, Cassano T, Denotti C, Devillanova FA, Isaia F, Lelj F, Lippolois V, Tommasi R (2003) J Phys Chem A 107:9679–9687
42. Bachler V, Olbrich G, Neese FK, Wieghardt KE (2002) Inorg Chem 41:4179–4193
43. Schläpfer CW, Nakamoto K (1975) Inorg Chem 14:1338–1344
44. Adams DM, Cornell JB, (1968) J Chem Soc A 1299–1303
45. Siimamann O, Fresco J (1971) Inorg Chem 10:297–302
46. Pokhodnya KI, Faulmann C, Malfant I, Andreu-Solano R, Cassoux P, Mlayah A, Smirno D, Leotin J (1999) Synt Met 103:2016–2019
47. Noodleman L (1981) J Chem Phys 74:5737–5743